Characterization of Aging Properties and Precipitation of Copper Base Alloys

Shigeo Sato[1,*], Kazuaki Wagatsuma[1], Minoru Isshiki[2], Hitoshi Tashiro[3] and Shigeru Suzuki[2]

[1] *Institute for Materials Research, Tohoku University, Sendai 980-8577, Japan*
[2] *Institute of Multidisciplinary Research for Advanced Materials, Tohoku University, Sendai 980-8577, Japan*
[3] *Formerly, Technical Development Bureau, Nippon Steel Co., Futtsu 293-8511, Japan*

(Received March 8, 2010 ; Final form April 28, 2010)

ABSTRACT

This article describes recent progresses in the microstructural characterization of precipitates in several copper base alloys and the mechanical and electrical properties of the alloys. To improve the strength and electrical conductivity of Cu-Ti and Cu-Ni-Si alloys, the effects of composition and cold-work treatment prior to aging treatment on these properties are examined. The properties of the alloys are found to be improved by precipitation during aging. The small-angle X-ray scattering method and X-ray absorption fine structure analysis are used for characterizing the precipitates formed. Our results show that there is an optimum size of precipitates for obtaining high strength, although the electrical conductivity monotonically increases with aging time. We also show that cold rolling after solution treatment is effective in increasing the strength and electrical conductivity of the alloys. We discuss the precipitation mechanism in the cold-rolled alloys on the basis of the experimental results.

Keywords: electrical conductivity, Vickers hardness, small-angle X-ray scattering, extended X-ray absorption fine structure, X-ray absorption near-edge structure

* E-mail: s.sato@imr.tohoku.ac.jp
Tel: +81-22-215-2133, Fax: +81-22-215-2131

1. INTRODUCTION

Copper base alloys are used as electrical interconnection materials as well as structural materials, because of their high electrical conductivity and strength. Copper-beryllium alloys have high electrical conductivity and strength; however, beryllium is toxic and may cause environmental pollution. This has led to the development of advanced copper base alloys and their processing. Cu-Ti and Cu-Ni-Si alloys are typical copper base alloys that exhibit precipitation hardening by aging treatment. The properties of these alloys can be improved by optimizing the addition of alloying elements and the process conditions. Although a number of studies on the mechanical properties and the microstructure of copper base alloys have been carried out thus far /1–10/, systematic changes in precipitation caused by aging treatment have not yet been studied.

This article presents a review on the effects of aging treatment on the electrical conductivity and the mechanical properties, and on the precipitation phenomena in high-purity Cu-Ti and Cu-Ni-Si alloys. The properties of Cu-Ti binary alloys and Cu-Ni-Si alloys, which were aged at 720 K after quenching, were measured at room temperature. To characterize the precipitation process in these aged alloys, the small-angle X-ray scattering (SAXS) method and X-ray absorption fine structure (XAFS) analysis were used. On the basis of these experimental results, the relationship between the properties and the precipitation is discussed, because the control of precipitates is

known to be an important factor to be considered while designing the alloy processes.

2. CHANGES IN PROPERTIES BY AGING TREATMENT

Cu-Ti and Cu-Ni-Si alloys were prepared from high-purity materials by the hydrogen plasma arc melting method. Then, they were shaped into samples for measurements. They were annealed at approximately 1173 K under vacuum and then quenched in oil at room temperature. Subsequently, the samples were isothermally aged at 720 K. The aging temperature was selected on the basis of changes in several properties by isochronal aging /5/. Details of sample preparation have been described elsewhere /5, 6/. In these studies, isothermal aging curves of electrical resistivity and Vickers hardness were obtained by alternating aging treatments at 720 K and measurements for these properties.

Figure 1 shows isothermal aging curves of the electrical resistivity for three samples that had different compositions: copper-1.3 at%, 2.6 at%, and 4.5 at% titanium alloys, which are hereafter referred to as Cu-1.3Ti, Cu-2.6Ti, and Cu-4.5Ti, respectively /6/. The electrical resistivity in an as-quenched state decreases with increasing the titanium composition. The relationship between the electrical resistivity and bulk titanium concentration in Cu-Ti alloys obtained in the present study was rather high, compared to those reported by Nagarjuna *et al.* /11/. The difference may be attributed to different quenching rates of samples in these two works, because the super-saturated amount of titanium principally determining the electrical resistivity may depend on the quenching rate.

The isothermal aging curves show that the electrical resistivity decreases with increasing aging time. This indicates that the amount of titanium dissolved in a copper matrix decreases and the precipitation of titanium compounds occurs during the aging. Although small variations in the electrical resistivity are detected during the aging treatment up to 500 s, primary decreases in the electrical resistivity start at an aging time of approximately 1000 s. It should be noted that the aging time in this main aging stage is almost independent of the bulk titanium concentration. This suggests that the effective density of the precipitates is almost independent of the bulk titanium concentration. This may be a characteristic of aging properties of the present alloys; the super-saturated amount of solutes generally affects the density of precipitates. It is also shown that the electrical conductivity of the aged alloys is denoted with IACS% (international annealed cupper standard), which is given by the ratio of the electrical resistivity of pure copper to that of an aged alloy.

Figure 2 shows the micro-Vickers hardness and the electrical resistivity of copper-3.1at% nickel-1.4at% silicon alloy (hereafter referred to as Cu-3.1Ni-1.4Si) as a function of aging time at 720 K /5/. Two different pretreatments were performed prior to the aging treatment. One of the pretreatments was solution treatment at approximately 1173 K (hereafter referred to as ST), and the other was cold rolling by 50% after the solution treatment (referred to as STCR). The aging curves show that the electrical resistivity decreases with increasing aging time, which is fundamentally similar to the behavior of Cu-Ti alloys. It should be noted that the resistivity of this alloy decreased considerably during isothermal aging. This is considered to be a result of the decrease in the amount of alloying elements dissolved in a copper matrix due to complete precipitation of Ni_2Si in Cu-3.1Ni-1.4Si. The aging time required to reach the maximum hardness is shortened due to the cold-rolling treatment, and the over-aging, where the hardness of the alloy decreases, is observed in the sample aged more than ca. 3×10^4 s. These aging characteristics can be possibly attributed to the coarsening of precipitates. The details of the precipitation behavior will be discussed in the next section.

To compare the properties of the Cu-Ti and Cu-Ni-Si base alloys with those of the other copper base alloys, the relationships between the tensile strength and IACS% for several copper base alloys are summarized as shown in **Figure 3** /12/, where the tensile strength of several copper alloys is converted from the hardness data. For comparison, the properties of a composite wire of high-strength steel cord coated with copper (Cu/Fe-C) are also plotted in **Figure 3**. The copper coating on the composite wire increased the electrical

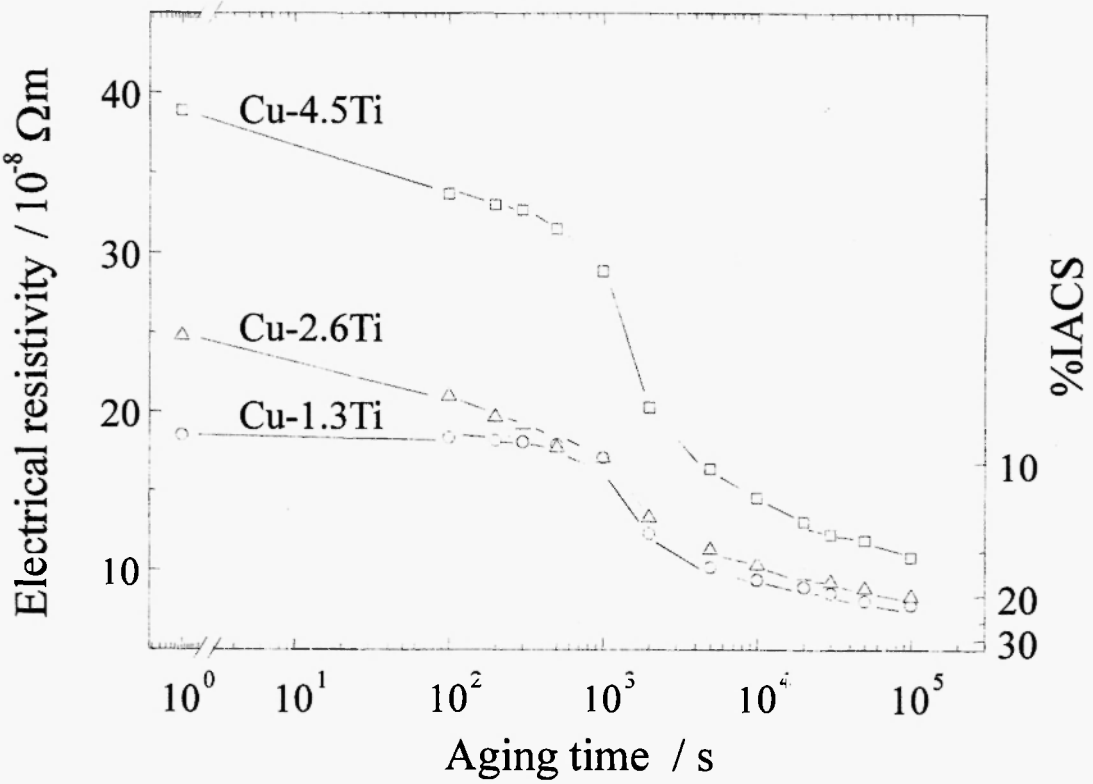

Fig. 1: Changes in electrical resistivity of Cu-Ti alloys by aging at 720 K /6/.

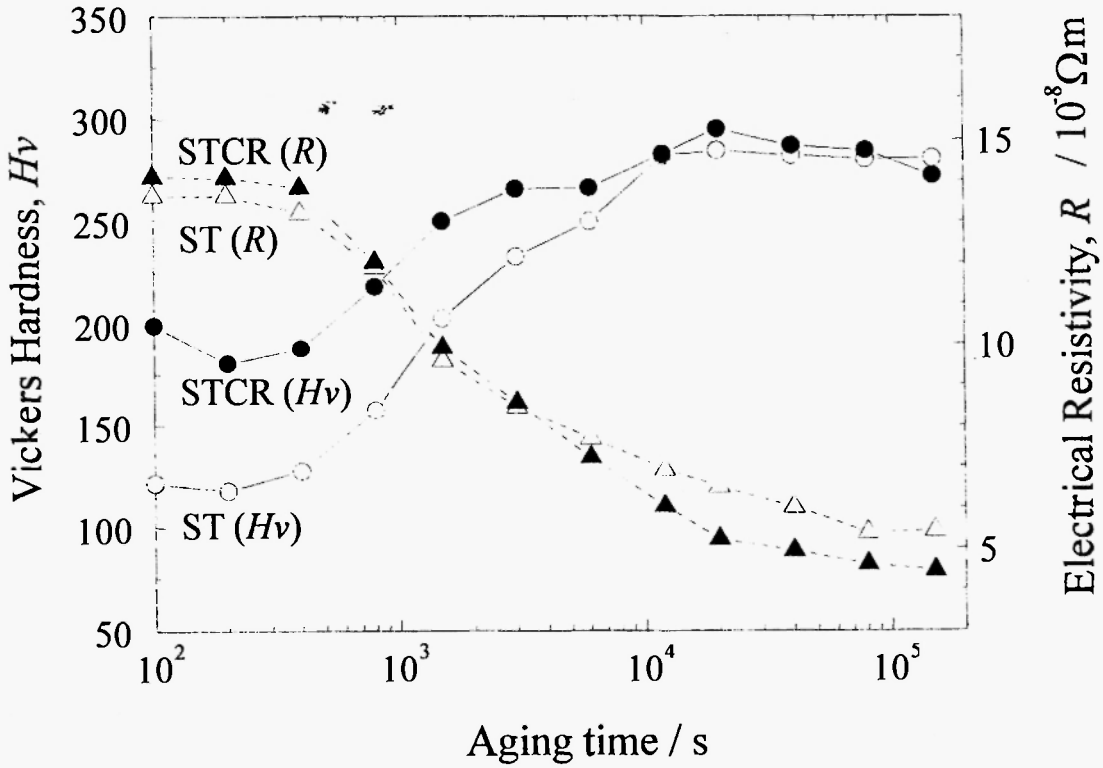

Fig. 2: Changes in hardness (circles) and electrical resistivity (triangles) of copper-3.1at% nickel-1.4at% silicon alloys that were as solution-treated (ST) and cold rolled (CR) after solution treatment (ST), i.e., STCR, by aging at 720 K /5/.

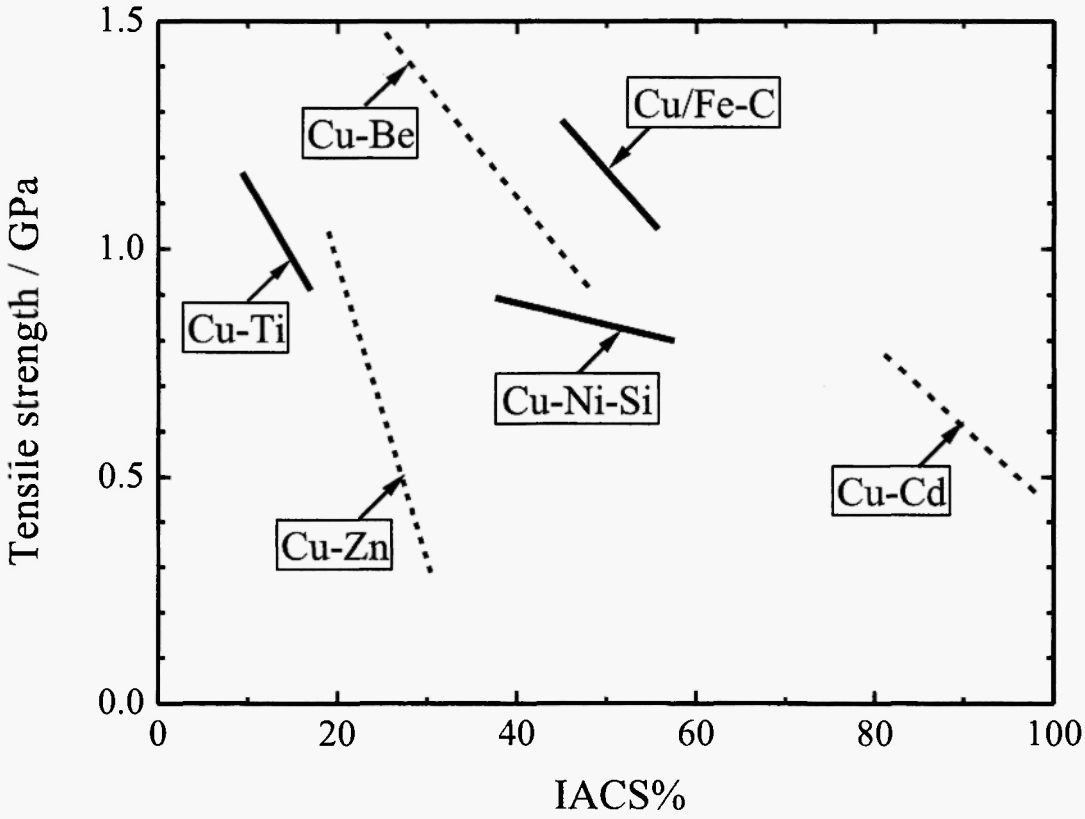

Fig. 3: Relationship between tensile strength and IACS% in several copper base alloys.

conductivity of the composite wire, while the strength of the composite wire was maintained due to the steel cord having a high tensile strength of approximately 3 GPa /13/. The electrical conductivity and the mechanical properties of such a composite were successfully improved by optimizing process conditions.

Although the properties of the copper base alloys were controlled not only by the species and the composition of the alloying elements but also by the process conditions, we were interested in the aging properties and precipitation in the Cu-Ti and Cu-Ni-Si alloys in this article. This is because these alloys exhibit typical precipitation processes as well as the aging properties, as shown in **Figures 1** and **2**.

3. CHARACTERIZATION OF PRECIPITATION USING X-RAY PROBE

3.1. Analysis of precipitation behavior using SAXS method

3.1.1. Dependence of size and number density of precipitates on composition of Cu-Ti alloys

The titanium composition in Cu-Ti alloys is of great importance in the formation of precipitates during the aging process /3, 6/. To understand how the titanium composition correlates with the size and the number density of precipitates, quantitative analysis using SAXS analysis is required. In the SAXS analysis, a monochromatic X-ray is incident on a sample, and the X-ray is scattered by electron density inhomogeneities

like precipitates in a copper matrix. The scattering occurs at all points in the precipitates, and the scattered X-rays interfere with each other. We observe the superposition of the interfered waves in small scattering-angle region. Since the SAXS signal is detected as the sum of a number of interfered waves for different distances between two points within the inhomogeneity, a SAXS profile shows a broad profile, which is discernible as a hump in a log(scattering intensity)–log(scattering angle) plot. The hump appears at a lower scattering angle with an increase in the size of the inhomogeneities and becomes broader with the spread of size distribution. These characteristics give us information on the size of precipitates in the copper matrix from the SAXS analysis.

Generally, the SAXS intensity can give the number density of precipitates by converting SAXS results into absolute units. However, it is difficult to extract weak SAXS signals from intense background scattering due to sample imperfections such as surface imperfections and crystal defects /14, 15/. However, we can convert the electrical resistivity of the alloy into the concentration of titanium dissolved in a copper matrix, because titanium dissolving in the copper matrix raises the electrical resistivity considerably. Thus, we can estimate the amount of titanium atoms in precipitates by measuring the electrical resistivity in Cu-Ti alloys. Re-estimation of the SAXS results by using the variation of the electrical resistivity can lead to the number density of the precipitates.

Figure 4 shows SAXS profiles of Cu-1.3Ti, Cu-2.6Ti, and Cu-4.5Ti /16/, which are described in Sec. 2, aged at 720 K, as a function of a magnitude of the scattering vector,

$$q = 4\pi\sin(\Theta/2)/\lambda, \quad (1)$$

where Θ is the scattering angle and λ is the wavelength of the X-rays.

In the SAXS profile of Cu-1.3Ti, a clear hump was observed only at an aging time of 2000 s because the quantity of precipitates would be low at shorter aging times. By contrast, humps in the SAXS profiles of Cu-2.6 and Cu-4.5Ti were discernible at aging times of 200, 500, and 1000 s and shift to the low-q side with the aging time. It is interesting that the position of the humps appearing in these SAXS profiles is almost independent of the titanium composition at each aging time, while the intensity of the humps increases with the titanium composition. This suggests that the titanium composition has an influence on the number density of the precipitates.

To evaluate the SAXS profiles, distance distribution functions (DDFs), $P(r)$, were calculated by fitting calculated SAXS profiles to the experimental ones using the indirect Fourier transformation (IFT) method /17/, as shown in **Figure 4**. A DDF gives a relative number of distances of two points inside a particle as a function of the distance; a peak position in the DDF represents a radius of a spherical particle. The precipitate radii, which are estimated from the DDFs, are shown in **Figure 5** /16/. In the case of Cu-2.6Ti and Cu-4.5Ti, the precipitate radii at aging times of 200 and 500 s were approximately 2 nm, irrespective of the titanium composition, and no growth of precipitates was observed up to an aging time of 500 s. At aging up to 2000 s, the radii of the precipitate increased up to approximately 3.5 nm, irrespective of the titanium composition. These results suggest that the growth rate of precipitates would not be significantly affected by the titanium composition.

In calculating the number density of precipitates, the phase of the precipitates needs to be defined. It has been reported that the precipitates formed by a moderate aging treatment are Cu_4Ti /18/. Therefore, the number of precipitates is estimated using the size of Cu_4Ti precipitates and the molar fraction of Cu_4Ti, which can be calculated from the electrical resistivity, as shown in **Figure 1.** The number of precipitates is calculated based on the assumption that Cu_4Ti precipitates are spherical. **Figure 6** shows the change in the number of precipitates with the aging time /16/. The number of precipitates for Cu-2.6Ti and Cu-4.5Ti increased in the initial aging stage up to 500 s. The gradual decrease in the electrical resistivity up to this aging time, as shown in **Figure 1**, was due to the increase in the formation of precipitates. From an aging time of 1000 s, the number of precipitates distinctly decreased, indicating the occurrence of Ostwald ripening of precipitates. Therefore, the growth of precipitates, which began from

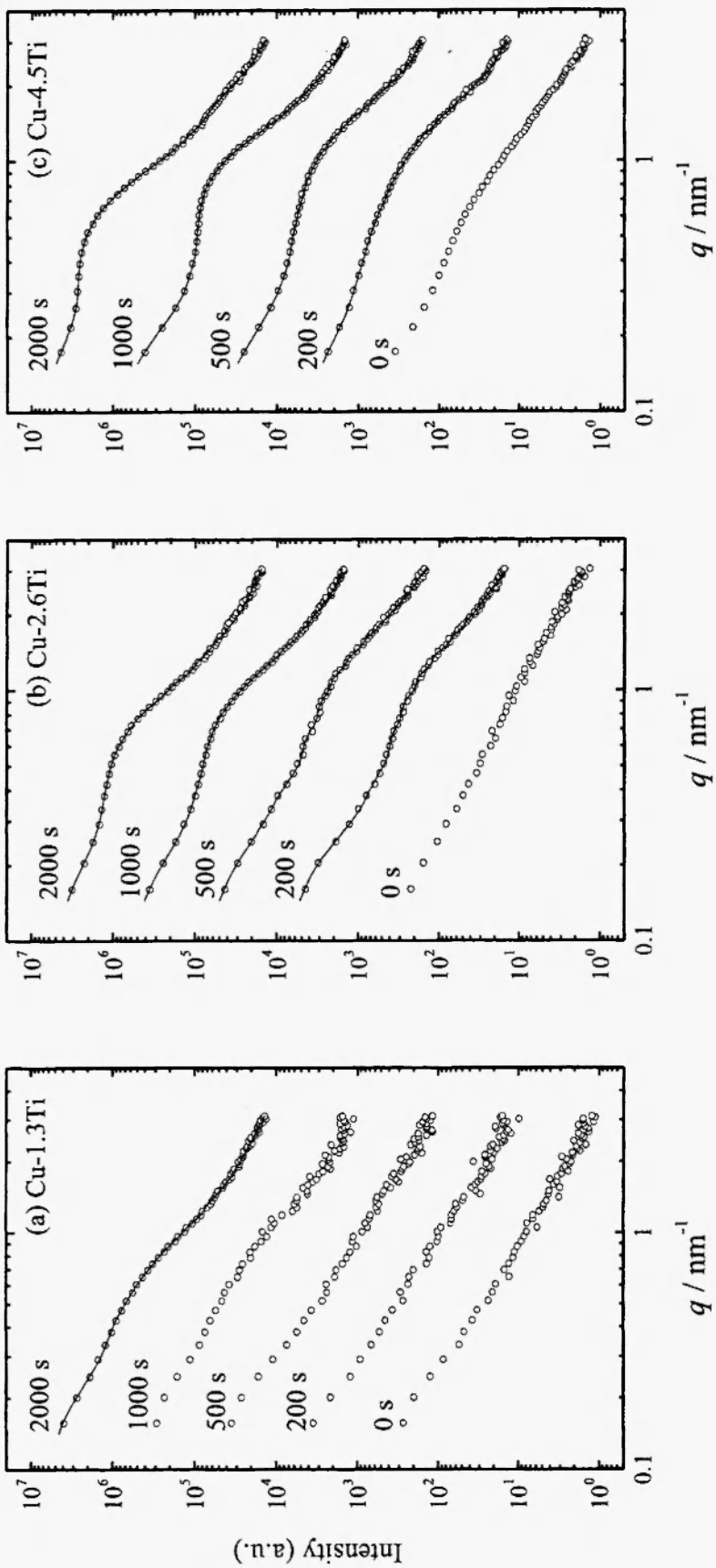

Fig. 4: SAXS profiles of (a) Cu-1.3Ti, (b) Cu-2.6Ti, and (c) Cu-4.5Ti aged for 0, 200, 500, 1000, and 2000 s /17/. The open circles and solid line denote the experimental and calculated curves, respectively.

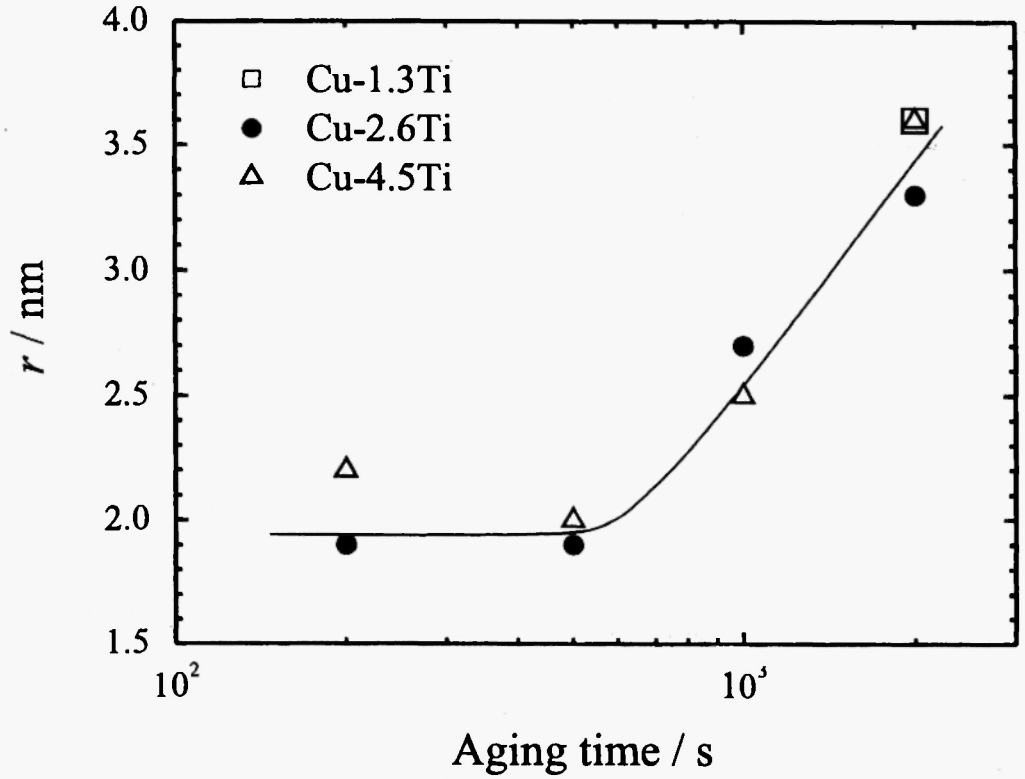

Fig. 5: Radius evolution of precipitates in Cu-1.3Ti, Cu-2.6Ti, and Cu-4.5Ti aged at 720 K /17/.

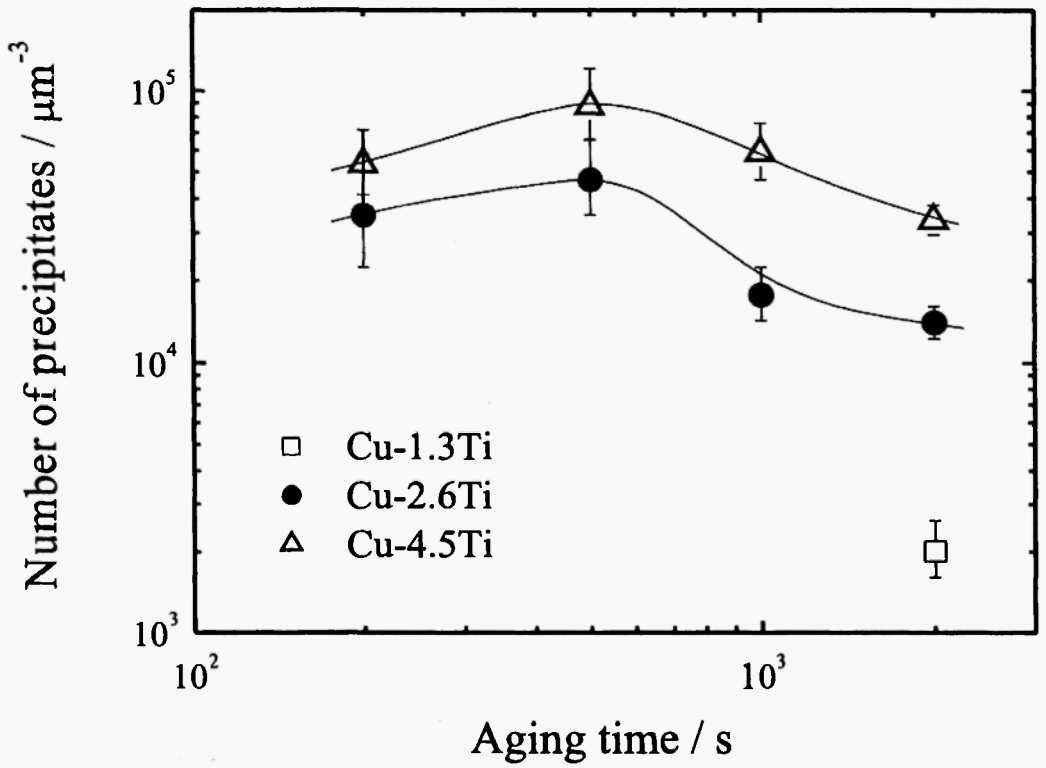

Fig. 6: Variations in number density of precipitates in Cu-Ti alloys with aging time /17/.

the aging time of 1000 s, was mainly brought about by the Ostwald ripening of the precipitates.

3.1.2. Effect of cold-rolling treatment and trace element addition on precipitation in Cu-Ni-Si alloys

A cold work treatment prior to an aging treatment leads to higher electrical conductivity and better mechanical properties after an adequate aging treatment, and reduces the aging time to attain peak hardness /5, 18–21/. These effects suggest that the cold work modifies the formation and growth behavior of precipitates. Besides the cold work, the addition of trace elements, such as iron and magnesium, into Cu-Ni-Si alloys can improve the strength and the electrical conductivity /5, 22/. It can be deduced that the addition of these elements in the alloys also modifies the growth behavior of precipitates. To understand these mechanisms, it is beneficial to characterize the growth behaviors of precipitates quantitatively using the SAXS method.

We conducted the SAXS analysis of Cu-Ni-Si alloys using our in-house facility /23/. However, because of the small difference in the scattering factors between nickel and copper, the SAXS signal from the precipitate (nickel silicide) in a copper matrix tended to be weak. Moreover, intense background signals from surface imperfections and crystal defects overlapped the SAXS signal. To overcome this problem, an anomalous scattering phenomenon, which changes the atomic scattering factor, could provide us an attractive solution by enhancing the scattering contrasts between the precipitates and the copper matrix. Whereas the difference in atomic scattering factors between nickel and copper is about 1 at X-ray energies far from the absorption edge of nickel, that difference increases to 4.4 at 8.313 keV, which is 20 eV below the nickel K-absorption edge. Thus, the following SAXS results for analyzing precipitates formed in Cu-Ni-Si alloys are based on the experimental data using the X-ray of 8.313 keV just below the nickel K-absorption edge.

Cu-3.1Ni-1.4Si, described in Sec. 2, was used for SAXS measurements. **Figures 7(a)** and **7(b)** show SAXS profiles of ST and STCR in the aged samples at 720 K for 0, 10^3, and 10^4 s as a function of a magnitude of the scattering vector. The alloys aged for 10^3 s were in an intermediate aging state, and the alloys aged for 10^4 s exhibited high strength as well as high electrical conductivity, as indicated in **Figure 2**. Although precipitates were not formed in the non-aged state, strong X-ray scattering was detected for ST and STCR. This scattering decreased monotonically in the log-log plot, indicating that large-scale inhomogeneities, which originated in surface imperfections and crystal defects, brought about this scattering. The SAXS profiles of ST aged for 10^3 s showed a hump at about 1 nm^{-1}, and the position of the hump shifted to a smaller value of scattering vector at an aging time of 10^4 s. These SAXS profiles indicate the evolution and growth of nanometer-size precipitates. The SAXS profiles of STCR aged for 10^3 s were similar to that of ST. However, the hump in the SAXS profile of STCR became unclear at an aging time of 10^4 s, suggesting that precipitates coarsened inhomogeneously.

To further advance this discussion, the calculated SAXS profiles were fitted to experimental ones, as shown in **Figure 7**, and DDFs were estimated. **Figure 8** shows the DDFs for the alloys aged at 720 K for 0, 10^3, and 10^4 s. The size distribution at the aging time of 0 s was less meaningful because the DDFs at this aging time were calculated from the background scattering. Although DDFs for aged alloys were calculated from the scattering profile, including the background scattering, clear peaks can be observed in the DDFs for the aged samples. At the aging time of 10^3 s, a clear peak appeared at about 2 nm in the DDFs for both ST and STCR. This suggests that the growth rate of precipitates is independent of the cold work up to this intermediate aging stage. The peak in the DDF for ST shifted to about 3 nm at the aging time of 10^4 s, indicating that precipitates grew in a single-modal size distribution. In contrast, the corresponding peak for STCR aged for 10^4 s was obscure. This indicates that precipitates formed in STCR aged for 10^4 s significantly coarsened in a multi-modal size distribution. Whereas the growth rate of precipitates for STCR was almost comparable to that for ST up to the intermediate aging stage, dislocations introduced by the cold work probably caused coarsening of precipitates at the prolonged aging

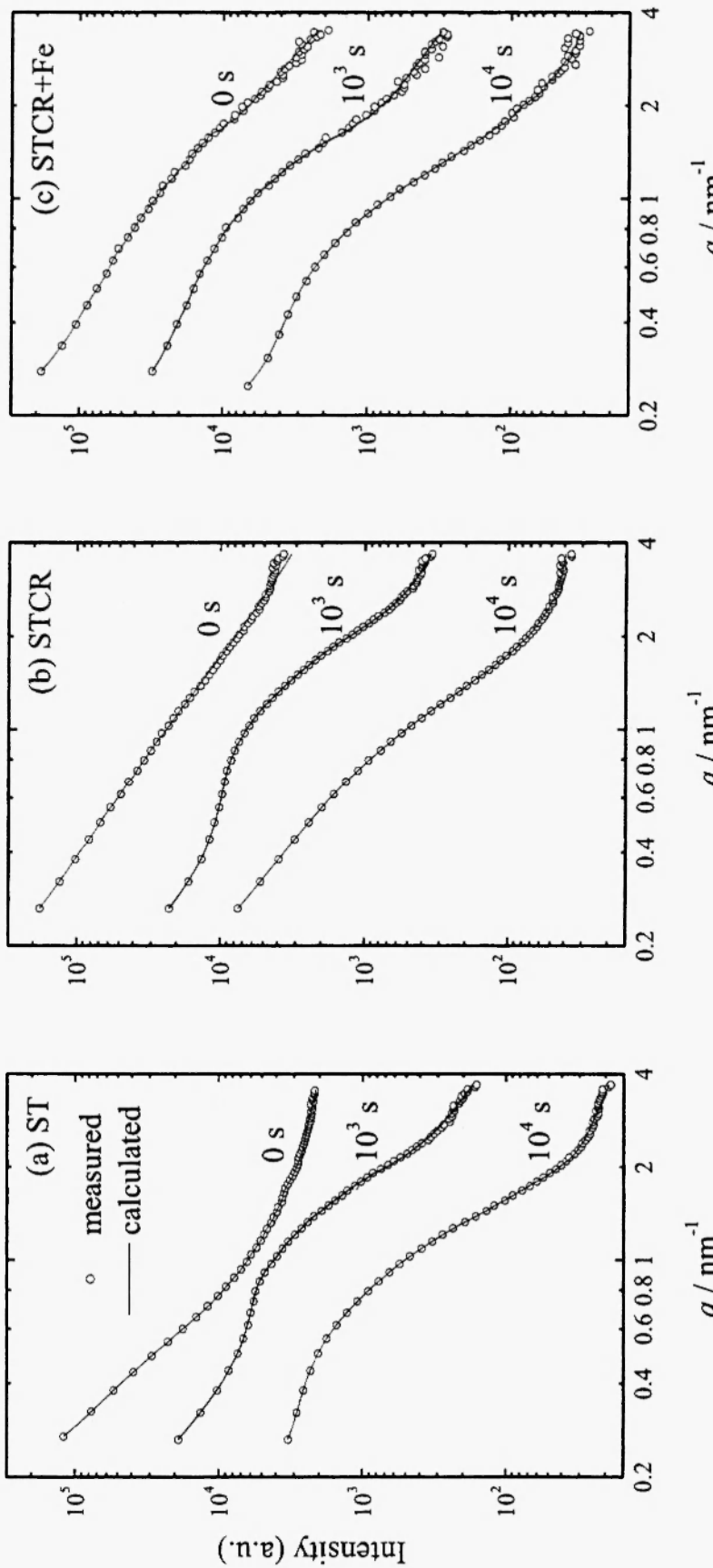

Fig. 7: SAXS profiles of (a) ST, (b) STCR, and (c) STCR+Fe aged at 720 K for 0, 10^3, and 10^4 s. The open circles and solid line denote the experimental and calculated curves, respectively.

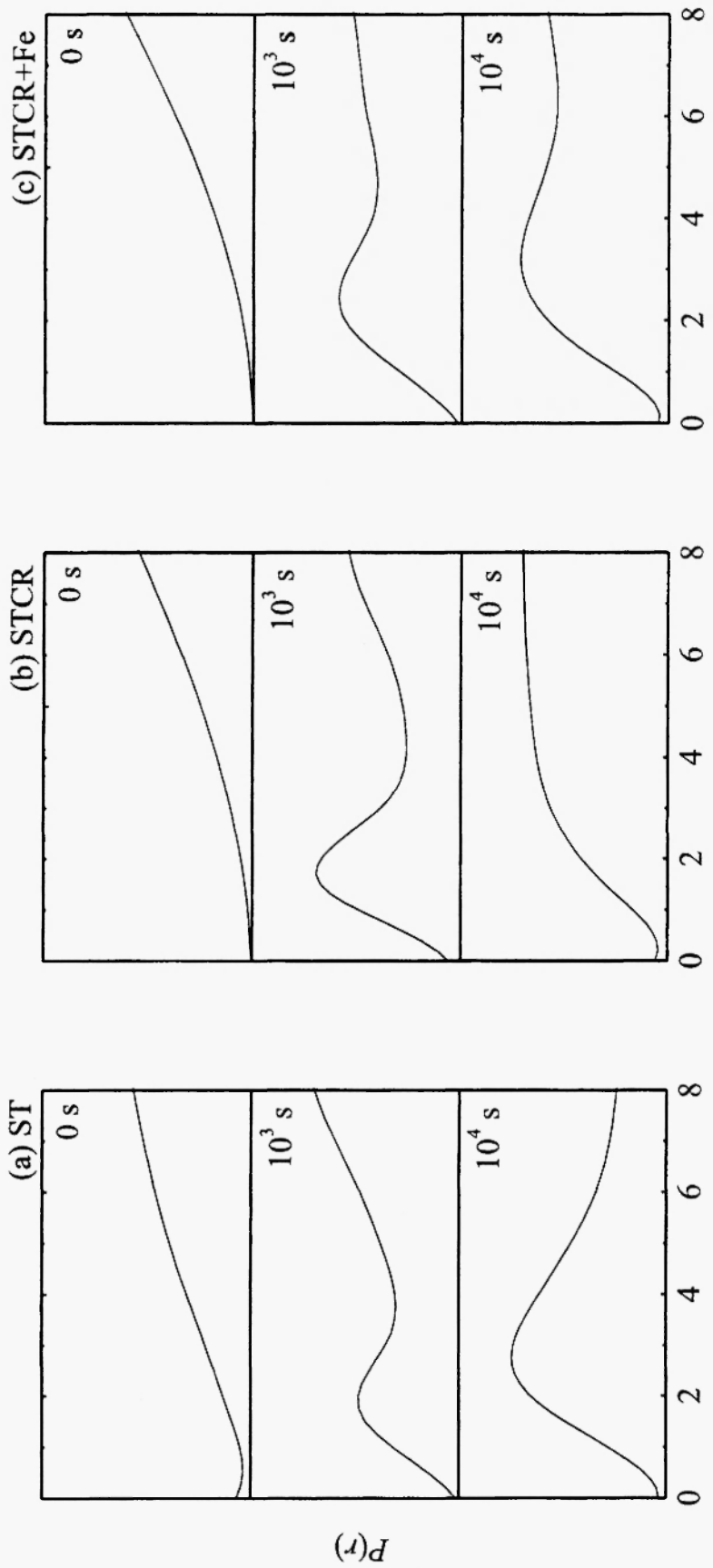

Fig. 8: DDFs, $P(r)$, representing size distribution of precipitates formed in (a) ST, (b) STCR, and (c) STCR+Fe aged at720 K for 0, 10^3, and 10^4 s.

time of 10^4 s. Further analysis is now conducting to understand aging behaviors of dislocations in the copper matrix using X-ray diffraction line profile analysis.

We also examined the Cu-3.0 at%Ni-1.3 at%Si-0.2 at%Fe alloy, which was solution-treated at 1173 K and subsequently cold rolled by 50% (STCR+Fe). Figure 7(c) shows SAXS profiles of STCR+Fe aged at 720 K for 0, 10^3, and 10^4 s. At the intermediate aging stage (10^3 s), the overall shape of the SAXS profile of STCR+Fe was similar to that of STCR. At an aging time of 10^4 s, however, while the hump in the SAXS profile of STCR was unclear, a clear hump remained in that of STCR+Fe. This indicates that precipitates in STCR+Fe grew homogeneously even up to the prolonged aging time of 10^4 s. **Figure 8(c)** shows the DDFs for STCR+Fe at aging times of 0, 10^3, and 10^4 s. The DDF at the aging time of 10^3 s had a peak around 2 nm in radius, which was consistent with that of STCR. However, in contrast to the DDF for STCR aged for 10^4 s, a clear peak remained around 3 nm in the DDF for STCR+Fe aged for 10^4 s. These results demonstrate that trace iron in Cu-Ni-Si alloys can suppress coarsening of precipitates.

3.2. Application of XAFS analysis to evaluation of precipitation

3.2.1. Characterization of local structures of solute elements in Cu-Ni-Si alloys using extended X-ray absorption fine structure analysis

As described in Sec. 3.1.2, trace iron in Cu-Ni-Si alloys has a desirable effect on precipitation growth. To understand the role of iron in the alloys, its atomic-level behavior during the aging process must be elucidated. An analytical technique for this is extended X-ray absorption fine structure (EXAFS) analysis, which can determine the local structure of solute elements in alloys. **Figure 9** shows k^3-weighted EXAFS functions at the Ni K- and Fe K-edges for STCR+Fe aged at 720 K for 0, 10^3, and 10^4 s /24/. At an aging time of 0 s, the Fe K- and Ni K-edge EXAFS functions were quite similar to the Cu K-edge EXAFS function of a copper foil. This clearly indicates that iron and nickel atoms were substitutionally dissolved in the fcc-Cu lattice. Characteristic shoulder peaks, appearing at around 60 and 75 nm^{-1} in the Ni K- and Fe K-edge EXAFS functions at an aging time of 0 s, were unclear at an aging time of 10^3 s. In addition, the Fe K-edge EXAFS function was almost identical to the Ni K-edge one during the aged states. These results imply that the environmental structure of nickel and iron is changed by the formation of precipitates and that the environmental structure of iron is the same as that of nickel. The EXAFS functions at an aging time of 10^4 s did not show any significant change, compared to those at the aging time of 10^3 s. The local atomic structure of nickel and iron would be almost completed by aging at least up to 10^3 s.

It has been reported that δ-Ni_2Si nucleation occurs for aged Cu-Ni-Si alloys with a composition around Ni:Si = 2:1 /25/. Therefore, precipitates formed in STCR+Fe are expected to be δ-Ni_2Si. Ni-K EXAFS functions for several nickel silicides were calculated using the FEFF code /26/. Since the calculated EXAFS function led by δ-Ni_2Si revealed a similar shape of the EXAFS functions for aged alloys, as shown in **Figure 9**, the precipitates formed in the present alloys were likely to be δ-Ni_2Si. It should be emphasized that the Fe K-edge EXAFS functions were identical to the Ni K-edge EXAFS functions, suggesting that iron atoms substituted nickel sites in δ-Ni_2Si. According to the SAXS analysis, the coarsening of the precipitates is suppressed in STCR+Fe. This indicates that δ-Ni_2Si in which iron is partially substituted with nickel would be thermally stabilized, resulting in retarding the dissolution of the δ-Ni_2Si precipitates during precipitate coarsening or Ostwald ripening in STCR+Fe.

Although the present structural data give us a new insight into the aging behavior of iron atoms, more EXAFS data from systematically prepared samples, such as iron composition and longer aging times with over-aging, are required to verify the role of trace iron in Cu-Ni-Si alloys in the growth behavior of precipitates. This structural study is ongoing.

3.2.2. Estimation of reaction rate of precipitation using X-ray absorption near edge structure spectra

X-ray absorption near edge structure (XANES) spectra are normally used for characterizing chemical

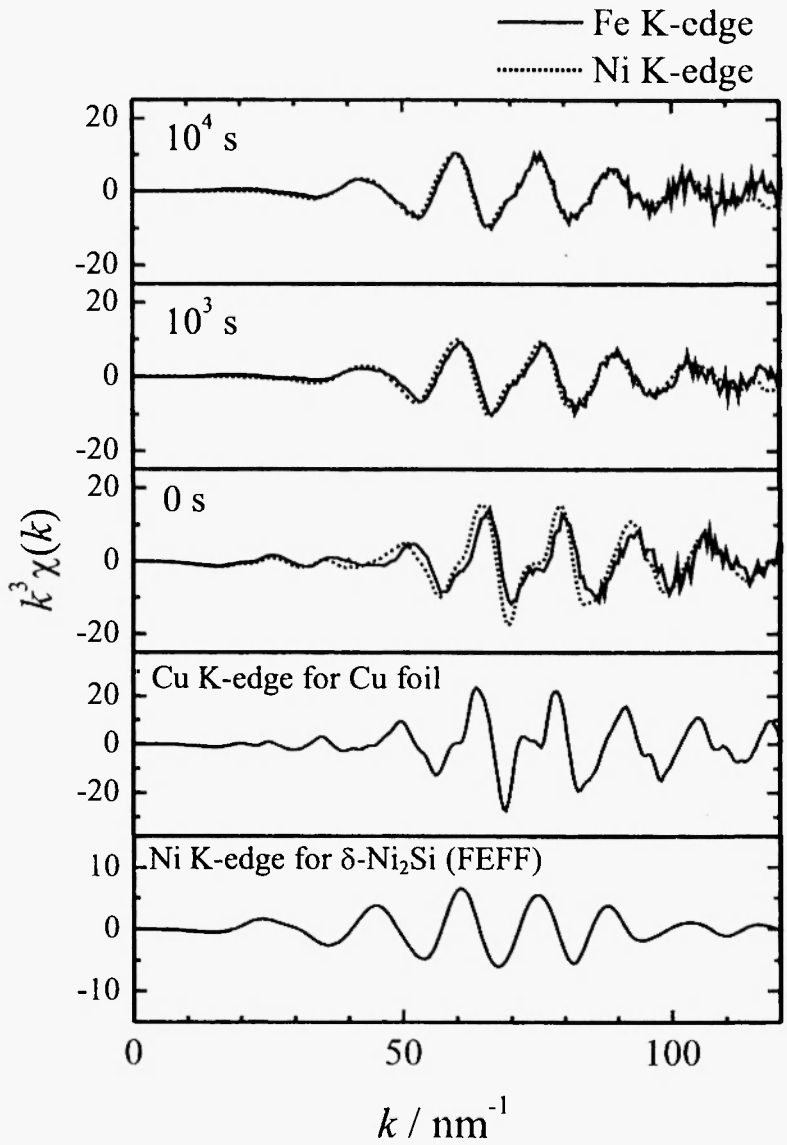

Fig. 9: Fe K-edge and Ni K-edge EXAFS functions of STCR+Fe /24/. The Cu K-edge EXAFS of a Cu foil and the calculated Ni K-edge EXAFS functions of δ-Ni_2Si are also shown for reference.

states of various compounds. The XANES spectra are also applicable to estimating the relative concentration in a mixture of compounds, because the intensity of a XANES spectrum is proportional to the molar ratio of each compound. Therefore, we used XANES spectra as a probe of precipitation rate.

ST and STCR of the Cu-3.1Ni-1.4Si alloy were evaluated using XANES spectra. The Ni K-edge XANES spectra of ST and STCR are shown in **Figure 10**. As suggested in Sec. 3.2.1, nickel in Cu-Ni-Si alloys is substituted in the fcc-copper lattice before aging treatment and is changed to δα-Ni_2Si by the following aging treatment. We confirmed this reaction from a variation of the XANES spectra with aging time. The dependence of XANES spectrum of STCR on the aging time was similar to that of the XANES spectrum of ST. This indicates that precipitation in STCR occurs in a similar manner to that of ST. Nevertheless, it should be noted that the variation of the spectrum for STCR was somewhat larger than that of ST at the aging time of 10^4 s, suggesting that silicide formation in STCR was more advanced than that in ST aged for 10^4 s. The

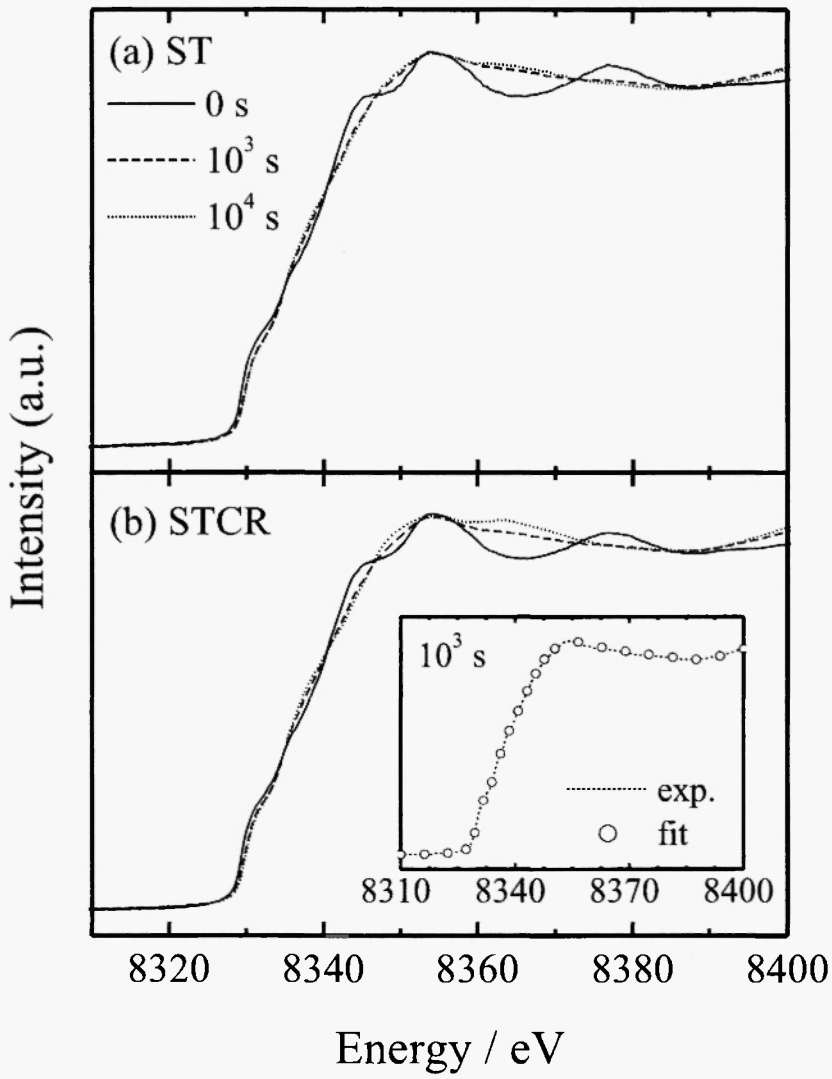

Fig. 10: Ni K-edge XANES spectra of (a) ST and (b) STCR at aging times of 0, 10^3, and 10^4 s. The inset in (b) shows an example of the fitting result for the XANES spectrum of STCR aged for 10^3 s.

nickel-silicide fraction of total nickel, α, in these alloys can be estimated by fitting a XANES spectrum of an aged sample, f_{aged}, with XANES spectra of non-aged, $f_{non\text{-}aged}$, and fully silicided, $f_{silicide}$, samples:

$$f_{aged} = (1-\alpha) f_{non\text{-}aged} + \alpha f_{silicide}. \quad (2)$$

In this study, however, the full formation of silicide was not achieved in any aged samples. Thus, the XANES spectrum of STCR aged for 10^4 s was used as a relative standard. As an example of this calculation fit, a fitted XANES spectrum of STCR aged for 10^3 s is shown in the inset of **Figure 10(b)**. The XANES spectrum of the aged sample fits well with Eq. (2). The fraction of nickel-silicide in total nickel of ST and STCR are shown in **Table 1**. Although the values in Table 1 are not absolute but relative values, several interesting features can be recognized. At the intermediate aging stage of 10^3 s, the nickel-silicide formation in ST and STCR proceeded at the same rate. This is consistent with the SAXS result that the precipitate size of STCR is comparable to that of ST at the aging time of 10^3 s. On the other hand, the nickel-silicide fraction of STCR was larger than that of

ST at the aging time of 10^4 s. This clearly suggests that the dislocation introduced by the cold work in the copper matrix prompted the nickel-silicide formation at the prolonged aging state (10^4 s), where the copper alloy was deficient in solute elements for precipitation. Such preferential precipitation in the cold-rolled sample could have caused significant decreased amounts of nickel and silicon dissolved in the copper matrix during the aging process, which may be attributed to improvement of the electrical conductivity in STCR.

Table 1
Fraction of nickel-silicide in total nickel in ST and STCR aged at two different aging times, (nickel-silicide fraction in STCR at aging time of 10^4 s is assumed to be 1).

Aging time / s	ST	STCR
10^3	0.73	0.74
10^4	0.86	1

4. CONCLUSION

This article presents recent research on the structural characterization of precipitates as well as the physical properties of Cu-Ti and Cu-Ni-Si alloy systems. The electrical conductivity of Cu-Ti alloys depends significantly on the concentration of titanium. However, with the progress of aging, the variations in the electrical conductivity, is almost independent of the titanium concentration of the solution-treated state. This feature would be originated from the similarity of the growth rate of precipitates. Our results also indicate that the onset aging time of Ostwald ripening is independent of the titanium concentration.

The hardness and electrical conductivity of aged copper alloys could be improved by cold-rolling treatment after solution treatment. Moreover, the addition of a small amount of iron in Cu-Ni-Si alloys was effective in improving these physical properties. The improvement in the physical properties was associated with nanometer-scale behaviors of solute elements during the aging process, as determined by using SAXS method. We verified that cold-rolling treatment can introduce dislocations in the copper matrix, which contributes to preferential precipitation. The trace iron in Cu-Ni-Si alloys could suppress to develop the coarsening of precipitates. We also showed that the XAFS analysis was suitable for evaluating the quantity of the formed silicide formation as well as the local structures of solute elements in copper alloys.

The analytical methods presented in this article can give us advanced insight into the precipitation behaviors of precipitate-hardenable alloys, and their application to other alloys such as aluminum- or iron-base alloy systems can be expected.

ACKNOWLEDGEMENTS

We would like to express gratitude to Prof. Y. Waseda for the fruitful discussions. This work was supported by a Grant-in-Aid for Scientific Research Fund from the Japan Society for Promotion of Science. The SAXS measurements using synchrotron radiation were performed at SPring-8 with the approval of National Institute for Materials Science (NIMS), (Proposal No. 2004B0090 / BL-15XU). The XAFS measurements using synchrotron radiation were performed at the same facility with the approval of Japan Synchrotron Radiation Research Institute (JASRI), (Proposal No. 2009A1110 / BL-01B1).

REFERENCES

1. S. Nagarjuna, M. Srinivas, K. Balasubramanian and D.S. Sarma, *Scr. Metall. Mater.* **33**, 1455–1460 (1995).
2. S. Nagarjuna, M. Srinivas, K. Balasubramanian and D.S. Sarma, *Acta Mater.* **44**, 2285–2293 (1996).
3. S. Nagarjuna, M. Srinivas, K. Balasubramanian and D.S. Sarma, *Mater. Sci. Eng. A*, **259**, 34–42 (1999).
4. S. Nagarjuna, K. Balasubramanian and D.S. Sarma, *Mater. Sci. Eng. A* **259**, 118–124 (2001).
5. S. Suzuki, N. Shibutani, K. Mimura, M. Isshiki and Yoshio Waseda, *J. Alloys and Compounds* **417**, 116–120 (2006).
6. S. Suzuki, K. Hirabayashi, H. Shibata, K. Mimura,

M. Isshiki and Y. Waseda, *Scr. Mater.* **48**, 431–435 (2003).
7. D. Zhao, Q.M. Dong, P. Liu, B.X. Kang, J.L. Huang and Z.H. Jin, *Mater. Sci. Eng. A* **361**, 93–99 (2003).
8. F. Huang, J. Ma, H. Ning, Y.W. Cao and Z. Geng, *Mater. Lett.* **57**, 2135–2139 (2003).
9. D.M. Zhao, Q.M. Dong, P. Liu, B.X. Kang, J.L. Huang and Z.H. Jin, *Mater Chem. Phys.* 79, 81–86 (2003).
10. P. Liu, J. Su, Q. Dong and H. Li, *Mater. Lett.* **59**, 3337–3342 (2005).
11. S. Nagarjuna, K. Balasubramanian and D.S. Sarma, *Mater. Sci. Eng. A* **22**, 118–124 (1997).
12. Y. Waseda ed., *"Metals Data Book", 4th ed.*, Japan Inst. Metals, Sendai, (2005), p.182.
13. H. Tashiro, T. Tarui, S. Sasaki, A. Yoshie, S. Nishida, S. Ohashi, K. Nakamura and H. Demachi, *Nippon Steel Technical Report* **80**, 38–43 (1999).
14. M. Roth, *J. Appl. Cryst.* **10**, 172–176 (1977).
15. P. Fratzl, Y. Yoshida and G. Vogl, *Phys. Rev. B* 46, 11323–11331(1992).
16. S. Sato, Y. Takahashi, T. Sanada, K. Wagatsuma and S. Suzuki, *J. Alloys Compds.* **477**, 846–850 (2009).
17. O. Glatter and O. Kratky, *Small-Angle X-ray Scattering*, Academic Press, London (1982), pp.131–136.
18. S. Nagarjuna, K. Balasubramanian and D.S. Sarma, *J. Mater. Sci.* **34**, 2929–2942 (1999).
19. R. Markandeya, S. Nagarjuna and D.S. Sarma, *Mater. Charact.* **54**, 360–369 (2005).
20. R. Markandeya, S. Nagarjuna and D.S. Sarma, *Mater. Sci. Eng. A* **404**, 305–313 (2005).
21. R. Markandeya, S. Nagarjuna and D.S. Sarma, *Mater Charact.* **57**, 348–357 (2006).
22. C. Watanabe, H. Hiraide, Z. Zhang and R. Monzen, *J. Soc. Mat. Sci., Japan* **54**, 717–723 (2005).
23. Y. Takahashi, T. Sanada, S. Sato, T. Okajima, K. Shinoda and S. Suzuki, *Mater. Trans.* **48**, 101–104 (2007).
24. S. Sato, Y. Takahashi, T. Sanada, K. Shinoda, K. Wagatsuma and S. Suzuki, *Adv. in X-ray Anal.*, **52**, 9–14 (2009).
25. R. Kainuma, K. Tamura, T. Miyamoto, I. Ohnuma and K. Ishida, *J. JRICu* **48**, 81–85 (2009).
26. A. L. Ankudinov, B. Ravel, J. J. Rehr and S. D. Conradson, *Phys. Rev. B* **58**, 7565–7576 (1998).